Formation of diamonds in laser-compressed hydrocarbons at planetary interior conditions

D. Kraus [1,2,3]*, J. Vorberger[1], A. Pak[4], N. J. Hartley [1,5], L. B. Fletcher[6], S. Frydrych[4,7], E. Galtier[6],
E. J. Gamboa[6], D. O. Gericke[8], S. H. Glenzer[6], E. Granados[6], M. J. MacDonald[6,9], A. J. MacKinnon[6],
E. E. McBride[6,10], I. Nam[6], P. Neumayer[11], M. Roth[7], A. M. Saunders[2], A. K. Schuster[1], P. Sun[6,12],
T. van Driel[6], T. Döppner[4] and R. W. Falcone[2,13]

The effects of hydrocarbon reactions and diamond precipitation on the internal structure and evolution of icy giant planets such as Neptune and Uranus have been discussed for more than three decades[1]. Inside these celestial bodies, simple hydrocarbons such as methane, which are highly abundant in the atmospheres[2], are believed to undergo structural transitions[3,4] that release hydrogen from deeper layers and may lead to compact stratified cores[5–7]. Indeed, from the surface towards the core, the isentropes of Uranus and Neptune intersect a temperature–pressure regime in which methane first transforms into a mixture of hydrocarbon polymers[8], whereas, in deeper layers, a phase separation into diamond and hydrogen may be possible. Here we show experimental evidence for this phase separation process obtained by in situ X-ray diffraction from polystyrene $(C_8H_8)_n$ samples dynamically compressed to conditions around 150 GPa and 5,000 K; these conditions resemble the environment around 10,000 km below the surfaces of Neptune and Uranus[9]. Our findings demonstrate the necessity of high pressures for initiating carbon–hydrogen separation[3] and imply that diamond precipitation may require pressures about ten times as high as previously indicated by static compression experiments[4,8,10]. Our results will inform mass–radius relationships of carbon-bearing exoplanets[11], provide constraints for their internal layer structure and improve evolutionary models of Uranus and Neptune, in which carbon–hydrogen separation could influence the convective heat transport[7].

Being composed of highly abundant elements, hydrocarbons are one of the most common chemical species throughout the Universe. A considerable amount exists inside giant planets, especially icy giants such as Neptune and Uranus, which are also being found in steadily increasing numbers in extrasolar planetary systems. Chemical processes involving hydrocarbons can participate in shaping the interior of these planets where gravity compresses mixtures of light elements to densities of several grams per cubic centimetre while the temperature reaches thousands of kelvins, resulting in thermal energies of the order of chemical bond energies and above[2]. Attempts have been made to investigate the structural transitions of such systems in the

laboratory by studying methane inside laser-heated diamond anvil cells and in shock experiments with gas guns[4,10,12,13]. In diamond anvil cells, evidence for dissociation and polymerization has been found at pressures of 10–50 GPa and below the carbon melting temperature[4,10], resulting in a heavy hydrocarbon fluid[8]. Similar structural transitions are expected to happen in various hydrocarbons under shock compression[6,12,13], and this led to the postulation of possible diamond precipitation inside the icy giants of our Solar System[1]. However, owing to the lack of in situ measurements in previous shock experiments, details of whether, when and how diamonds can be created are not fully understood.

Some hints of diamond formation have been reported for methane samples in laser-heated diamond anvil cells at pressures of 10–50 GPa and temperatures above 2,000 K (ref. [4]), and for pressures of 10–80 GPa and temperatures above 3,000 K (ref. [10]); other experiments found that pure carbon appeared in the form of graphite or diamond at 10–80 GPa and temperatures between 1,000 K and 1,500 K, but a stable fluid of heavy hydrocarbons at higher temperatures[8]. All this is in contrast to theoretical studies with atomistic simulations, which predict that much higher pressures are required for dissociation and phase separation of hydrocarbons into diamond and hydrogen[3,14,15] ($\gtrsim$190 GPa at 2,000 K and $\gtrsim$300 GPa just above 0 K). The findings from diamond anvil cells may suffer from an externally forced demixing process, as atomic or molecular hydrogen is readily absorbed by the diamond anvils[16] and the metal gasket surrounding the sample[10]. Moreover, these metal gaskets, as well as pressure standards and laser absorbers included in the sample material, are known to lower the temperature threshold for hydrocarbon dissociation[17]. The big differences between the results for diamond anvil cells suggest that the observed chemical reactions are mainly influenced by the specific mix of materials in contact with the sample material for each case.

In contrast, dynamic shock experiments on hydrocarbons both compress and heat samples on very short timescales (approximately nanoseconds with lasers, microseconds with gas guns), reaching conditions similar to those investigated in diamond anvil cells. Moreover, shock experiments allow the creation of isolated systems that do not

[1]Helmholtz-Zentrum Dresden-Rossendorf, Bautzner Landstrasse 400, 01328 Dresden, Germany. [2]Department of Physics, University of California, Berkeley, CA 94720, USA. [3]Institute of Solid State and Materials Physics, Technische Universität Dresden, 01069 Dresden, Germany. [4]Lawrence Livermore National Laboratory, Livermore, CA 94550, USA. [5]Open and Transdisciplinary Research Institute, Osaka University, Suita, Osaka 565-0871, Japan. [6]SLAC National Accelerator Laboratory, Menlo Park, CA 94309, USA. [7]Institut für Kernphysik, Technische Universität Darmstadt, Schlossgartenstrasse 9, 64289 Darmstadt, Germany. [8]Centre for Fusion, Space and Astrophysics, Department of Physics, University of Warwick, Coventry CV4 7AL, UK. [9]University of Michigan, Ann Arbor, MI 48109, USA. [10]European XFEL GmbH, Holzkoppel 4, 22869 Schenefeld, Germany. [11]GSI Helmholtzzentrum für Schwerionenforschung GmbH, Planckstrasse 1, 64291 Darmstadt, Germany. [12]Department of Physics, Stanford University, Stanford, CA 94305, USA. [13]Lawrence Berkeley National Laboratory, Berkeley, CA 94720, USA. *e-mail: d.kraus@hzdr.de
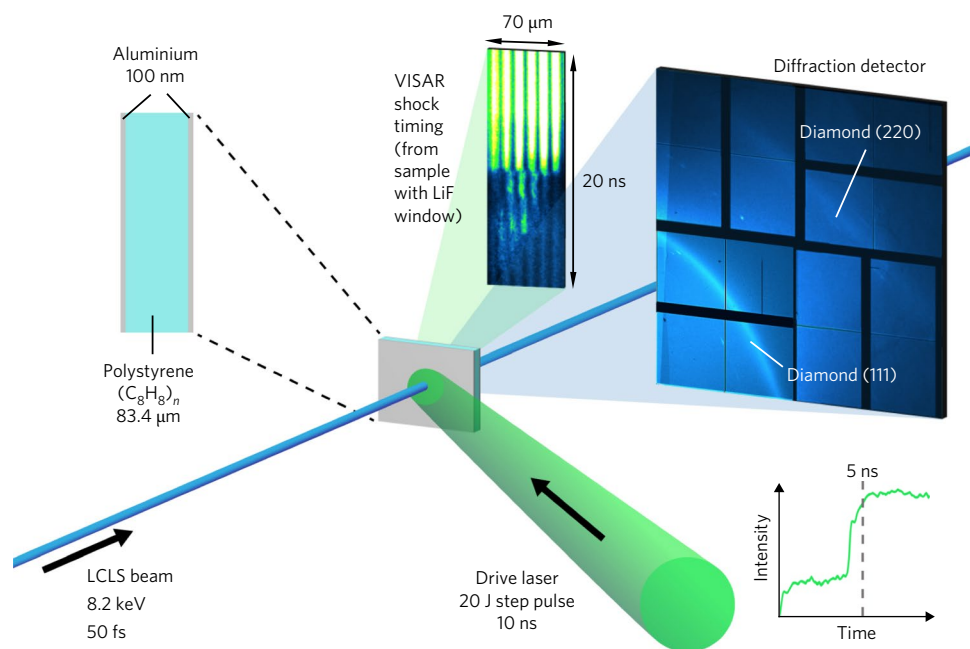
Fig. 1 | Schematic of the experimental set-up at the Matter at Extreme Conditions end-station of the LCLS. Two high-energy laser beams of different intensity and arrival time are overlaid to form a step pulse, which drives two shock compression waves into a polystyrene film. The shock waves are timed with a VISAR[21] to coalesce at the rear side of the sample. The microscopic state is probed by a single X-ray pulse with 8.2-keV photon energy and 50-fs pulse duration. X-ray diffraction is recorded by a large-area X-ray detector, which clearly shows the formation of diamond during the second compression stage. Remnants of the aluminium coating result in a weak and spotty diffraction pattern that can clearly be distinguished from the emerging diamond rings. The colour in the bottom left quadrant of the detector image has been scaled to provide good contrast for both observed diamond diffraction rings.

chemically interact with the surroundings, owing to the short time-scale of the experiment. In aiming to study hydrocarbon dissociation and diamond formation at higher pressures, comparable to the deeper interiors of giant planets, the difficulty in shock compression is to keep the temperature below the diamond melting line[18], because of the shock-induced entropy increase. Nevertheless, this can be achieved by using a sequence of shocks instead of a single shock. Our approach uses a laser-driven two-stage shock compression of polystyrene $(C_8H_8)_n$ up to pressures around 150 GPa, for which the temperature is expected to remain below 6,000 K. The microscopic structure is then probed in situ by ultrafast X-ray diffraction[19].

The experiment reported here was performed at the Matter in Extreme Conditions end-station of the Linac Coherent Light Source (LCLS) at Stanford National Accelerator Laboratory[20]. The available combination of high-energy lasers ($\gtrsim$10 J per pulse) with an X-ray free-electron laser allows for femtosecond X-ray diffraction to directly access the kinetics of shock-induced chemistry. A schematic of the experiment is shown in Fig. 1. The polystyrene sample is compressed by a step-pulse laser profile, adjusted for optimal sample conditions by using the in situ X-ray diffraction data as well as a velocity interferometer system for any reflector (VISAR)[21] that provides additional timing constraints when a lithium fluoride (LiF) window is mounted on the rear side of the sample by determining the exact moment of the shock release and the corresponding velocity of the polystyrene/LiF interface (see Methods). The initial drive intensity of $(2.7\pm0.3)\times10^{12}$ W cm^{-2} lasts for 4.5 ns before being raised to $(7.1\pm0.8)\times10^{12}$ W cm^{-2}. This results in two stages of shock compression that create conditions similar to planetary interiors at 150 GPa. A single shock compression producing the same final pressure would instead lead to temperatures well above the melting line of diamond and higher than predicted in the interior of the icy giants in our Solar System.

One-dimensional hydrodynamic simulations of the two-step shock compression using the HELIOS hydrodynamic code[22] are illustrated in Fig. 2. The drive intensity used in the simulations is adjusted to the shock timing observed in the experiment and compares well with the measured laser energies (2.25×10^{12} W cm^{-2} and 6.7×10^{12} W cm^{-2} were applied for the two steps). The first shock has a transit time of 7.6 ns while the second forms when the drive laser reaches maximum intensity and enters the pre-shocked dense material around 6 ns after the start of the laser drive. The two shocks then coalesce at the rear side 1.5 ns later. Using the SESAME 7590 equation of state (EOS) for polystyrene[23], which gives a good fit to measurements of the Hugoniot pressure–density relationship and of brightness temperature in this regime[24], we obtain a bulk density of (3.0 ± 0.1) g cm^{-3}, a temperature of $(5,000\pm500)$ K and a pressure of (150 ± 15) GPa as average conditions in the double-shocked material. This closely resembles the predicted environment at about 10,000 km into the interiors of Neptune or Uranus[9,25]. The reported uncertainties refer to the spatial and temporal gradients observed in the simulations. Available EOS tables for polystyrene are well constrained by precision gas gun and laser shock experiments on the Hugoniot relation in this regime[24] and do not show significant deviations at the moderately off-Hugoniot conditions accessed in our experiment (SESAME 7590 and SESAME 7592 have been tested). Moreover, we find that the interface velocities recorded with the VISAR are in reasonable agreement with the hydrodynamics simulations (see Methods and Supplementary Information).

Plots of in situ X-ray diffraction intensity (line-outs) at various time delays are shown in Fig. 3 for the experiment that corresponds to the described simulations. At ambient conditions, clear signatures of the amorphous polystyrene are observed together with various weak Bragg reflections from the aluminium coating on both sides. When launching the initial shock wave into the sample, half of the aluminium coating immediately vanishes as the front layer is vaporized and ablated by the laser drive. At the same time, the ambient amorphous diffraction features start to decrease as the compression waves travel through the sample. The first shock creates a
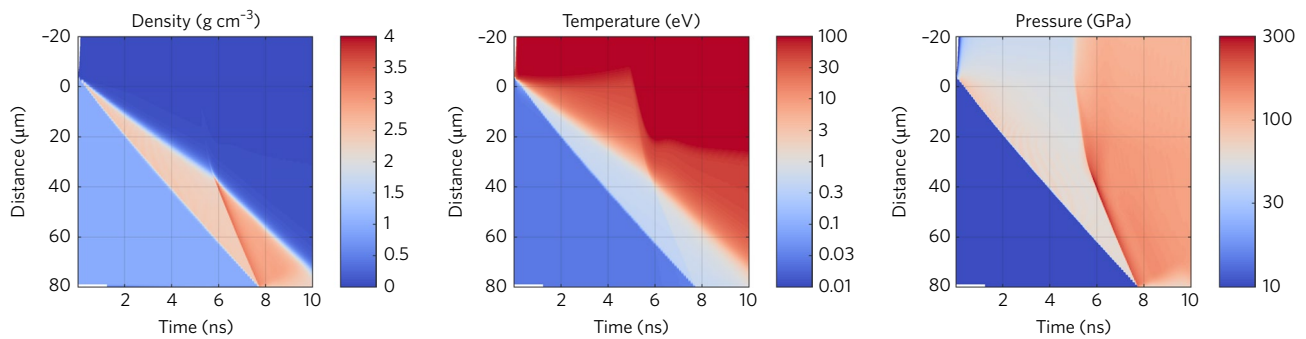
Fig. 2 | Hydrodynamic simulations of the two-stage shock compression. The colour plots show simulation results for mass density (left), temperature (centre) and pressure (right) for both compression stages. The drive laser hits the sample from the top in all diagrams, and the double-stage drive results in two time-delayed shock compression waves. The second shock reaches the dense pre-compressed part of the sample about 6 ns after the first compression wave, and both shocks coalesce at 7.6 ns when reaching the sample rear side. At this time, relatively homogeneous conditions of $\rho = (3.0 \pm 0.1)\,\mathrm{g\,cm^{-3}}$, $T = (5,000 \pm 500)\,\mathrm{K}$ and $P = (150 \pm 15)\,\mathrm{GPa}$ are predicted in the compressed sample material.

compressed C–H liquid, which results in a broad correlation peak centred around 3 Å⁻¹. In good agreement with the hydrodynamic simulations, which predict that the second shock enters the dense pre-shocked material about 6 ns after the start of the laser drive, we find the onset of new diffraction features at 6.2 ns. These peaks are compatible with the (111) and (220) Bragg reflections of compressed diamond at a density of $(4.14 \pm 0.06)\,\mathrm{g\,cm^{-3}}$ and grow until 7.4 ns, when the two shock fronts approach the rear surface. The density decrease due to the shock release shifts the broad liquid correlation peak towards lower wavenumber k. The diamond particles also decompress, and at 14.4 ns, the diffraction signature is compatible with diamond at ambient density. The overall diamond diffraction strength decreases at late times, which may be explained by diamond particles leaving the small corridor that is probed by the X-rays as a result of the 30° angle between X-rays and the sample's surface normal, or by partial decomposition of the decompressed diamonds in a hydrogen-rich environment.

The width of the (111) diffraction peak allows a lower limit of the diamond particle size to be inferred by means of the Scherrer formula[26]. We find an average full-width at half-maximum of 0.17 Å⁻¹ (2.9°) for the (111) reflection, which implies diamonds of at least 4 nm in diameter. Because defects and spatial density gradients also result in peak broadening, the actual size of the diamond particles is likely to be slightly larger. We do not observe any signature of diamond when applying just a single shock compression drive (shock pressures between 50 GPa and 180 GPa have been applied to the sample). In this case, the compressed polystyrene remains in an amorphous, complex liquid[27] or dense plasma state.

Diamond is also produced when slightly varying the laser intensity of the two compression stages: $(1.7 \pm 0.2) \times 10^{12}\,\mathrm{W\,cm^{-2}}$ followed by $(6.4 \pm 0.7) \times 10^{12}\,\mathrm{W\,cm^{-2}}$ ('low-pressure drive') and $(3.2 \pm 0.3) \times 10^{12}\,\mathrm{W\,cm^{-2}}$ followed by $(8.0 \pm 0.8) \times 10^{12}\,\mathrm{W\,cm^{-2}}$ ('high-pressure drive') were applied. These lead, respectively, to reduced pressure and temperature conditions of $(139 \pm 15)\,\mathrm{GPa}$, $(4,200 \pm 500)\,\mathrm{K}$, and to increased pressure and temperature conditions of $(159 \pm 15)\,\mathrm{GPa}$, $(6,100 \pm 500)\,\mathrm{K}$, according to hydrodynamic simulations in which the drive intensity was adjusted relative to the changes described above. Figure 4a shows typical diamond (111) diffraction peaks for the three two-step compression conditions. We infer average diamond densities of $(4.05 \pm 0.07)\,\mathrm{g\,cm^{-3}}$ for the low-pressure drive and $(4.23 \pm 0.05)\,\mathrm{g\,cm^{-3}}$ for the high-pressure drive.

The inferred density of the observed diamond particles can be applied as a valuable consistency check for the predictions from the hydrodynamic simulations. Using a recent multiphase EOS for carbon[28] that is benchmarked by first-principles simulations and well constrained by experiments, we obtain $P = 139\,\mathrm{GPa}$ for

$\rho = 4.14\,\mathrm{g\,cm^{-3}}$ and $T = 5,000\,\mathrm{K}$, consistent with the hydrodynamic simulations within the given error bars for density, temperature and pressure. This EOS results in 118 GPa for the low-pressure
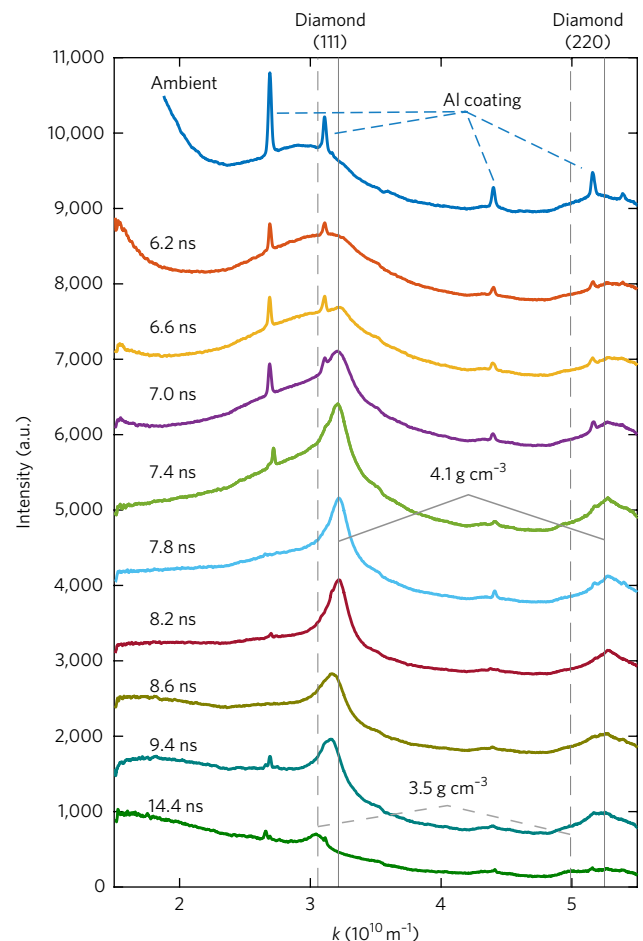

Fig. 3 | Diffraction line-outs. The diffraction signals of cold undriven samples show the typical features of amorphous polystyrene together with Bragg reflections from the aluminium coatings on the front and rear side. After the second shock wave has entered the pre-compressed sample, a strong diffraction signature of compressed diamond starts to appear. This feature remains after the shock release and shows decompression of the diamond particles to ambient density.
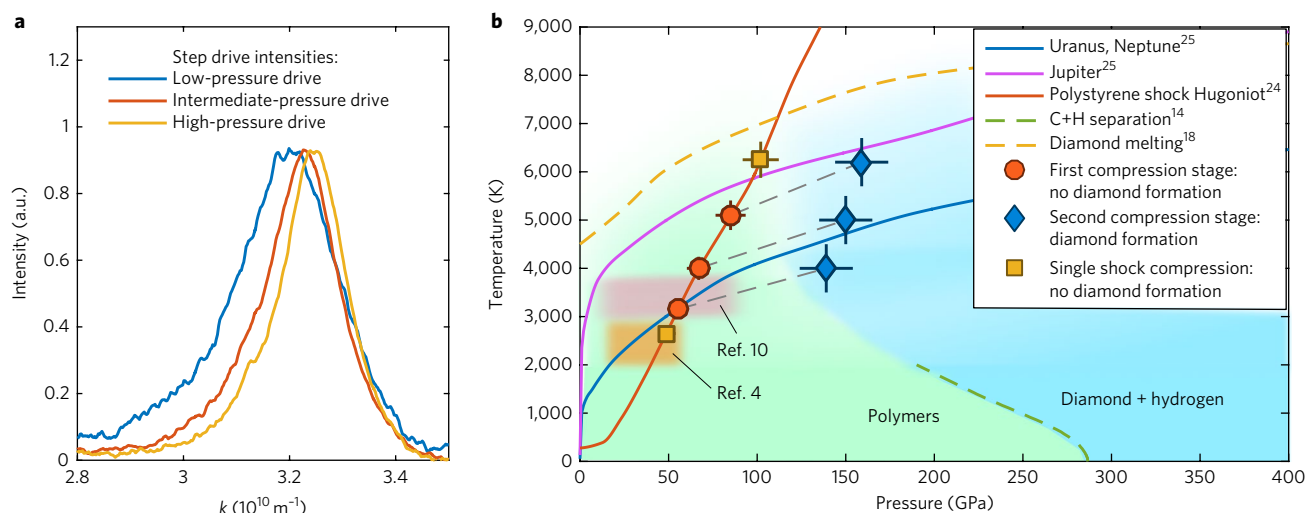
Fig. 4 | Summary of diamond formation. a, With increasing pressure and thus diamond density, the diamond (111) reflection moves to higher k. The broad background from remaining liquid polystyrene is subtracted for better comparison. **b**, The temperature and pressure conditions at which diamond formation is observed overlap with the predicted isentropes of Uranus and Neptune (represented by only one curve due to the small differences[25]) as well as Jupiter[25]. At the same time no trace of diamond is found when applying a single shock on polystyrene, which intersects the regime for which diamond formation was suggested by experiments[4,10] in diamond anvil cells (pink shading[4] and orange shading[10]). This supports the trend given by atomistic simulations[14], which predict the phase separation only at higher pressures. The error bars are given by spatial and temporal gradients in the hydrodynamic simulations, which are substantiated by several experimental cross-checks (see Methods and Supplementary Information).

drive condition and 165 GPa for the high-pressure drive condition. Although the latter is very close to the hydrodynamic simulations, the result for the low-pressure drive condition shows a larger discrepancy, but still provides consistency within the stated uncertainties (see Supplementary Information).

Figure 4b compares our results with planetary models, atomistic simulations of the carbon–hydrogen phase separation and previous experiments with diamond anvil cells. We do not observe any evidence of diamond formation on the probed section along the shock Hugoniot relation for polystyrene, which partially overlaps with the region of the phase diagram covered by experiments with diamond anvil cells. Moreover, we do not find that diamond formation mainly scales with temperature above a pressure threshold of ∼10 GPa, as reported in previous work[10]. Instead, in our experiment, diamond is observed only after compression by the second shock wave at pressures in excess of 100 GPa. In all three cases of two-step compression, the second shock raises the pressure by a factor of 2–3 but increases the temperature by only about 20%.

This pressure dependence is more in line with atomistic modelling and therefore suggests that the non-isolated nature of samples tested in diamond anvil cells may obscure conclusions about the carbon–hydrogen phase separation inside planets. In general, our results support the idea of carbon–hydrogen demixing and subsequent diamond precipitation inside hydrocarbon-bearing giant planets, where the temperature remains below the diamond melting line[18], but imply that it probably requires higher pressures than suggested by previous experimental work. This is important for planetary models because carbon–hydrogen demixing can result in a layer with reduced convection. Comparable to what is proposed to happen inside Saturn owing to hydrogen–helium demixing[29], this may considerably reduce the internal heat transport in the icy planets of our Solar System. Moreover, a layer structure due to carbon–hydrogen demixing will result in jumps in the mass–radius relationship of exoplanets with large amounts of methane[11]. Lower demixing pressures reduce the planetary mass at which this jump to larger radii will occur. Consequently, our results point to lower threshold masses than presented in the study of ref. [11], in which the authors assume demixing pressures between 170 GPa and 300 GPa,

and certainly much larger threshold masses than suggested by the diamond anvil cell experiments that we have discussed. Overall, our measurements underline the importance of chemical processes for evolutionary models of icy giant planets and that chemistry needs to be considered for a detailed understanding of mass–radius relationships, which are essential for constraining the material constituents and thus the general classification of exoplanets.

The timescales of diamond anvil cell experiments (seconds) are very different from dynamic laser compression experiments (nanoseconds), and both experimental methods are far from quantum molecular dynamics simulations (picoseconds) or planetary timescales (millions of years). Therefore, future experiments should aim for precise information on the kinetics of the demixing and phase separation processes to allow extrapolations that can better constrain models for the internal structure and evolution of methane-rich planets. Nevertheless, chemistry that can already be observed in short-timescale experiments will certainly happen on planetary timescales.

In addition to their relevance for planetary modelling, by showing the formation of diamonds that are possibly a few nanometers in size from laser-irradiated plastic, our results may identify a new method to produce diamond nanoparticles for material science and industrial applications[30].

Methods

Laser-driven double-stage shock compression. The samples were laser-cut out of a high-purity polystyrene film (initial density $\rho_0 = 1.046 \, g \, cm^{-3}$, 83.4 µm thick) and coated with 100 nm of aluminium on both front and rear sides. The compression was achieved by using two pulsed high-energy lasers (527 nm, 10-ns pulse duration, 200-µm focal spot diameter, smoothed with random phase plates). The two beams were set to flat-topped pulse shapes with different pulse energies and timing with respect to the X-ray probe in order to create the desired two-stage shock compression drive. For the 'intermediate-pressure drive', the initial laser pulse was at an energy of 8 J, with the subsequent 16-J pulse reaching its maximum intensity 5 ns after the initial pulse. Online pulse shape and energy measurements for each shot recorded a shot-to-shot energy fluctuation of less than 10%. The timing of the two shock waves, which is in very good agreement with the timing of the observed X-ray diffraction features, was additionally constrained by the VISAR system using samples with single-crystal lithium fluoride (LiF) windows at the rear side. With this method, the plastic/LiF interface velocity could be monitored at the moment when a shock front reached the rear side of the plastic samples.

A relatively low interface velocity implies that the initial shock reaches the rear side first, whereas a high velocity is clearly connected to the stronger shock overtaking the initial wave before reaching the rear side of the sample. Supplementary Fig. 1 illustrates VISAR raw data for a single shock driven by an 8-J flat-topped pulse as well as data for the double-shock drive described previously (8 J and 16 J). The velocity per VISAR fringe (VPF) is given by[31]

$$VPF = \frac{\lambda c}{4h(n - 1/n)(1 + \delta)(1 + \Delta\nu/\nu_0)}$$ (1)

where λ is the wavelength of the laser applied in the VISAR system (532 nm), c is the speed of light, h is the etalon thickness (for unambiguous velocity determination, two interferometers, VISAR 1 and VISAR 2, were used with different etalon thicknesses: VISAR 1, 8.09 mm; and VISAR 2, 5.08 mm), n is the index of refraction of the applied etalon material (1.4607 for ultraviolet-grade fused silica), δ accounts for the dispersion in the etalon (0.0318 for 532 nm and fused silica[31]) and $\Delta\nu/\nu_0$ accounts for the index of refraction in the shock-compressed window[32] (~0.28 for LiF at 100–200 GPa). We obtain VPF = 4.81 km s^{-1} for VISAR 1 and VPF = 7.66 km s^{-1} for VISAR 2. Supplementary Fig. 2 provides the inferred polystyrene–LiF interface velocities. In the case of a single shock, the recorded shock transit time of (7.8 ± 0.2) ns gives an average shock velocity of (10.7 ± 0.3) km s^{-1}, which corresponds to (65 ± 5) GPa according to the Hugoniot relation for polystyrene, which is highly constrained in this pressure regime[24]. For the polystyrene–LiF interface velocity, we obtain (4.2 ± 0.2) km s^{-1}. Using the equations for shock impedance matching[33] in combination with the well-constrained LiF Hugoniot relation[32] allows for inferring the pressure in the initial shock and we obtain (58 ± 7) GPa. This fits well to the hydrodynamic simulations, which yield (66 ± 7) GPa in this case. The comparison to the result from the transit time measurement implies that the shock is only slightly decaying with propagation. For the double-shock case, we obtain (6.4 ± 0.3) km s^{-1} for the polystyrene–LiF interface velocity. This corresponds to a shock pressure of (230 ± 20) GPa at the polystyrene–LiF interface. Both interface velocity and pressure compare very well to the hydrodynamic simulations shown in Fig. 2 with an attached LiF window (see Supplementary Fig. 3). The other drives described here ('low-pressure drive' and 'high-pressure drive') were realized with 6 J and 11.5 J, respectively, in the first pulse, followed by 16 J again in the second pulse. In these cases, the shocks are not optimally timed to coalesce at the rear side. However, clear diamond formation is also recorded, starting at the instant when the second shock is expected to enter the dense pre-shocked material.

Without the LiF window at the rear side, the VISAR just records a strong drop in reflectivity at shock breakout, but no fringe shift, owing to rapid evaporation and disassembly of the reflective 100-nm-thick aluminium coating. During the X-ray shots, LiF windows were not used, to avoid obscuring diffraction signals as well as avoiding damage to the X-ray detectors due to strong single-crystal reflections. The spatial and temporal resolution of the VISAR diagnostic also allows for assessing planarity and the steadiness of the shock waves. We find a reasonably planar shock release at the sample rear side in a 50-μm region. Moreover, particularly for the timed double-shock drive, the polystyrene–LiF interface velocity remains relatively constant within the planar region of the shock release for a few nanoseconds, which implies reasonably steady shocks in agreement with the very constant position of the diamond (111) diffraction feature before shock release. The same streak cameras as used for the VISAR system were used to determine the arrival time of the drive laser, by scattering its beams from the exact position of sample interaction into the VISAR system.

Ultrafast X-ray diffraction. The polystyrene samples were probed by using the LCLS X-ray free electron laser (XFEL) beam in self-amplified spontaneous emission mode (8.2-keV photon energy, 0.3% spectral bandwidth, 50-fs pulse duration, 20-μm spot size, approximately 3 mJ per pulse corresponding to 2×10^{12} photons per pulse). Using imprints of the X-rays in the aluminium coating on the sample rear side that is monitored by the VISAR diagnostic on each shot, an accuracy of 20 μm or better could be achieved for the spatial overlap of X-rays and the drive lasers. The timing of the X-ray pulse relative to the drive laser was chosen to probe the sample slightly before or exactly at the moment when the shock waves coalesce at the end of the plastic samples. X-ray diffraction was measured by a Cornell–Stanford Pixel Array detector (CSPAD)[34] of dimensions 8 × 8 cm^2 at a distance of 8.7 cm from the sample, covering diffraction angles from 18° to 99° above the XFEL beam axis. In this way, perturbing effects due to the horizontal polarization of the X-ray beam could be avoided. Angular calibration for the recorded 2θ range was obtained by diffraction of CeO$_2$ and LaB$_6$ powder samples. The diffraction line-outs presented here are corrected for non-sensitive regions of the CSPAD, geometrical differences in detector irradiance and the horizontal polarization of the incident X-rays. Noise caused by firing the drive laser is negligible. We only show line-outs up to 85° (5.6 Å^{-1}), because, for larger angles, scattered X-rays are mostly absorbed by the sample mount or the sample itself.

Data availability. The data that support the plots within this paper and other findings of this study are available from the corresponding author upon reasonable request.

References

1. Ross, M. The ice layer in Uranus and Neptune—diamonds in the sky? *Nature* **292**, 435–436 (1981).
2. Guillot, T. Interiors of giant planets inside and outside the Solar System. *Science* **286**, 72–77 (1999).
3. Ancilotto, F., Chiarotti, G. L., Scandolo, S. & Tosatti, E. Dissociation of methane into hydrocarbons at extreme (planetary) pressure and temperature. *Science* **275**, 1288–1290 (1997).
4. Benedetti, L. R. et al. Dissociation of CH$_4$ at high pressures and temperatures: diamond formation in giant planet interiors? *Science* **286**, 100–103 (1999).
5. Hubbard, W. B., Nellis, W. J., Mitchell, A. C., Limaye, S. S. & McCandless, P. C. Interior structure of Neptune: comparison with Uranus. *Science* **253**, 648–651 (1991).
6. Chau, R., Hamel, S. & Nellis, W. J. Chemical processes in the deep interior of Uranus. *Nat. Commun.* **2**, 203 (2011).
7. Nettelmann, N. et al. Uranus evolution models with simple thermal boundary layers. *Icarus* **275**, 107–116 (2016).
8. Lobanov, S. S. et al. Carbon precipitation from heavy hydrocarbon fluid in deep planetary interiors. *Nat. Commun.* **4**, 2446 (2013).
9. Helled, R., Anderson, J. D., Podolak, M. & Schubert, G. Interior models of Uranus and Neptune. *Astrophys. J.* **7**, 15 (2011).
10. Hirai, H., Konagai, K., Kawamurab, T., Yamamotob, Y. & Yagic, T. Polymerization and diamond formation from melting methane and their implications in ice layer of giant planets. *Phys. Earth Planet. Inter.* **174**, 242–246 (2009).
11. Helled, R., Podolak, M. & Vos, E. Methane planets and their mass–radius relation. *Astrophys. J. Lett.* **805**, L11 (2015).
12. Nellis, W. J., Ree, F. H., van Thiel, M. & Mitchell, A. C. Shock compression of liquid carbon monoxide and methane to 90 GPa (900 kbar). *J. Chem. Phys.* **75**, 3055–3063 (1981).
13. Nellis, W. J., Hamilton, D. C. & Mitchell, A. C. Electrical conductivities of methane, benzene, and polybutene shock compressed to 60 GPa (600 kbar). *J. Chem. Phys.* **115**, 1015–1019 (2001).
14. Gao, G. et al. Dissociation of methane under high pressure. *J. Chem. Phys.* **133**, 144508 (2010).
15. Sherman, B. L., Wilson, H. F., Weeraratne, D. & Militzer, B. Ab initio simulations of hot dense methane during shock experiments. *Phys. Rev. B* **86**, 224113 (2012).
16. Uzan-Saguy, C. et al. Diffusion of hydrogen from a microwave plasma into diamond and its interaction with dopants and defects. *Diamond Related Mater.* **11**, 316–322 (2002).
17. Ahmed, S., Abdullah, A., Rahman, F., Al-Dawood, A. & Al-Muhaish, F. Decomposition of hydrocarbons to hydrogen and carbon. *Appl. Catal. A* **359**, 1–24 (2009).
18. Wang, X., Scandolo, S. & Car, R. Carbon phase diagram from ab initio molecular dynamics. *Phys. Rev. Lett.* **95**, 185701 (2005).
19. Kraus, D. et al. Nanosecond formation of diamond and lonsdaleite by shock compression of graphite. *Nat. Commun.* **7**, 10970 (2016).
20. Glenzer, S. H. et al. Matter under extreme conditions experiments at the Linac Coherent Light Source. *J. Phys. B* **49**, 092001 (2016).
21. Barker, L. M. & Hollenbach, R. E. Laser interferometer for measuring high velocities of any reflecting surface. *J. Appl. Phys.* **43**, 4669–4675 (1972).
22. MacFarlane, J. J., Golovkin, I. E. & Woodruff, P. R. HELIOS-CR: A 1-D radiation–magnetohydrodynamics code with inline atomic kinetics modeling. *J. Quant. Spectrosc. Radiat. Transfer* **99**, 381–397 (2006).
23. Lyon, S. P. & Johnson, J. D. SESAME: The Los Alamos National Laboratory Equation of State Database. LANL Report No. LA-UR-92-3407 (1992).
24. Barrios, M. A. et al. High-precision measurements of the equation of state of hydrocarbons at 1–10 Mbar using laser-driven shock waves. *Phys. Plasmas* **17**, 056307 (2010).
25. Guillot, T. & Gautier, D. Giant planets. *Treatise Geophys.* **10**, 439–464 (2007).
26. Scherrer, P. Bestimmung der Größe und der inneren Struktur von Kolloidteilchen mittels Röntgenstrahlen. *Gött. Nachr.* **2**, 98 (1918).
27. Kraus, D. et al. Probing the complex ion structure in liquid carbon at 100 GPa. *Phys. Rev. Lett.* **111**, 255501 (2013).
28. Benedict, L. X. et al. Multiphase equation of state for carbon addressing high pressures and temperatures. *Phys. Rev. B* **89**, 224109 (2014).
29. Püstow, R., Nettelmann, N., Lorenzen, W. & Redmer, R. H/He demixing and the cooling behavior of Saturn. *Icarus* **267**, 323–333 (2016).
30. Mochalin, V. N., Shenderova, O., Ho, D. & Gogotsi, Y. The properties and applications of nanodiamonds. *Nat. Nanotech.* **7**, 11–23 (2012).
31. Celliers, P. M. et al. Line-imaging velocimeter for shock diagnostics at the OMEGA laser facility. *Rev. Sci. Instrum* **75**, 4916–4929 (2004).
32. Rigg, P. A., Knudson, M. D., Scharff, R. J. & Hixson, R. S. Determining the refractive index of shocked [100] lithium fluoride to the limit of transmissibility. *J. Appl. Phys.* **116**, 033515 (2014).

33. Forbes, J. W. *Shock Wave Compression of Condensed Matter* (Springer, Berlin/Heidelberg, 2012).
34. Herrmann, S. et al. CSPAD-140k: a versatile detector for LCLS experiments. *Nucl. Instrum. Methods Phys. Res. A* **718**, 550–553 (2013).

Author contributions
D.K., R.W.F., J.V., T.D., A.P., S.H.G., D.O.G., M.R., E.Ga., E.Gr., P.N. and A.J.M. were involved in the project planning. D.K., E.Ga., N.J.H., A.P., T.D., P.N., E.E.M., A.M.S., S.F., L.B.F., P.S., M.J.M., E.J.G., E.Gr., I.N. and T.v.D. carried out the experiment. Experimental data were analysed and discussed by D.K., J.V., N.J.H., A.K.S., S.H.G., D.O.G., A.P., E.E.M. and T.D. The manuscript was written by D.K., J.V., A.P., N.J.H., M.J.M., D.O.G. and T.D.

Competing interests
The authors declare no competing financial interests.

Additional information
Supplementary information is available for this paper at doi:10.1038/s41550-017-0219-9.

Reprints and permissions information is available at www.nature.com/reprints.

Correspondence and requests for materials should be addressed to D.K.

Publisher's note: Springer Nature remains neutral with regard to jurisdictional claims in published maps and institutional affiliations.